Spin-driven ferroelectricity and large magnetoelectric effect in monoclinic $MnSb_2S_4$

Chandan De,[1] N. V. Ter-Oganessian,[2] and A. Sundaresan[1,*]

[1]*Chemistry and Physics of Materials Unit and School of Advanced Materials, Jawaharlal Nehru Centre for Advanced Scientific Research, Jakkur P.O., Bangalore 560064, India*

[2]*Institute of Physics, Southern Federal University, Rostov-on-Don 344090, Russia*

(Received 12 March 2018; revised manuscript received 31 October 2018; published 26 November 2018)

We report a spin-driven ferroelectricity below the helical spin ordering temperature in a nonoxide mineral $MnSb_2S_4$, which crystallizes in a centrosymmetric monoclinic $HgBi_2S_4$ structure. At T∼25 K, the dielectric constant shows an anomaly and the spontaneous electric polarization begins to develop. The polarization obtained from pyroelectric current measurement can be switched by reversing the direction of poling electric field. Interestingly, upon applying magnetic field parallel to the electric field, the polarization is enhanced nearly six times above a critical field $H||E \sim 5$ T, demonstrating large magnetoelectric effect in this system. Below T∼25 K, this compound is known to exhibit an unusual magnetic structure where the spiral spins lie in the ac plane but propagate along the b axis with an angle of ∼133° between the adjacent magnetic moments. The origin of ferroelectric ordering has been attributed to the inverse Dzyaloshinskii-Moriya type interaction in accordance with local symmetry considerations.

DOI: 10.1103/PhysRevB.98.174430

I. INTRODUCTION

In recent years there has been an enormous interest in the emergent phenomena arising in strongly correlated systems in condensed matter physics [1,2]. One such phenomenon is the giant magnetoelectric effect or the multiferroicity where the electric and magnetic orders coexist with a strong cross coupling. This renders the manipulation of magnetic ordering by the electric field or vice versa and thus attracted tremendous interest from the academic as well as technological fields [3–6]. However, it has been a challenging task to find multiferroic materials due to certain symmetry restrictions. It requires that materials with both spatial inversion and time reversal symmetries are broken in order for them to have multiferroic properties. Among the various known multiferroics, the materials with ferroelectricity induced by magnetism have received much attention because of relatively strong coupling between magnetic and electric ordering [7,8]. The most exciting discovery was the observation of spin induced multiferroicity in the orthorhombic perovskite $TbMnO_3$ [9]. Here, the competing magnetic interactions arising from nearest (J_1) and next-nearest (J_2) neighbors results in a cycloidal magnetic ground state, which breaks the inversion symmetry and induces the electric polarization as explained via spin-current model and inverse Dzyaloshinskii-Moriya (DM) interaction model [10,11]. Subsequently, it has been observed that a frustrated magnetic structure often results in cycloidal magnetic ordering leading to a macroscopic electric polarization as observed in CuO, certain types of hexaferrites, $MnWO_4$, $Ni_3V_2O_8$, etc. [12–15]. The frustration can also lead to other spin structures such as E-type spin ordering where collinear up-up-down-down spins drive the ferroelectric distortion through a symmetric exchange interaction [16]. Another intriguing frustrated spin induced multiferroicity was found in a triangular lattice antiferromagnet with a proper screw type magnetic structure with 120° spin rotation angle. It is commonly thought that this spin structure cannot induce polarization according to the spin-current or exchange-striction models and an alternate model of spin dependent d-p hybridization is usually proposed based on the covalency between transition metal d and ligand p orbitals, which is modulated depending on the local spin moment direction via relativistic spin orbit interaction [17,18]. For example, in delafossite $CuFeO_2$, a proper screw spin order in a triangular lattice with $R\bar{3}m$ structure allows electric polarization. According to the symmetry restriction it was anticipated that the occurrence of d-p hybridization induced polarization may be observed in low crystal symmetry, e.g., triclinic, monoclinic, or rhombohedral [18]. Such examples are delafossite (ABO_2) (e.g., $CuCrO_2$, $AgCrO_2$) [19], MI_2 (M = Mn, Ni) [20] with CdI_2 structure and $RFe_3(BO_3)_4$ with $R32$ structure [21]. Later, it was suggested that electric polarization induced by proper screw spin structures in $CuFeO_2$ and $CuCrO_2$ can be explained by a general form of inverse DM type interaction, i.e., proportional to the vector product of two neighboring spins [22]. While most of the spin-induced multiferroics are oxide materials, only a few transition metal chalcogenides have been reported to exhibit multiferroic behavior [23–26].

The mineral clerite (named after Onisim Yegorovich Kler) $MnSb_2S_4$ crystallizes in the monoclinic ($C2/m$) $HgBi_2S_4$ type structure containing chains of manganese ions in octahedral coordination and the MnO_6 octahedra share their edges along the b axis. These chains are interlinked along the a axis through a distorted square pyramid of the Sb ions and form layers parallel to the c axis [27]. From the electronic band structure calculations based on local spin density approximation, an antiferromagnetic ground state was found to

*sundaresan@jncasr.ac.in

be energetically favorable [28,29]. Further, the magnetization measurements confirmed antiferromagnetic ordering below 25 K. Interestingly, a former neutron diffraction study has established an incommensurate helical spin structure where manganese magnetic moments lie in the *ac* plane. Along the chains of MnS_6 octahedra (*b* axis), the angle between adjacent spin is ∼133°, while it is 66.85° along the *a* axis, and collinear along the *c* axis [27]. Therefore, this spin structure can be considered as a screw type where the propagation vector lies along the spin chain (*b* axis). This type of spin structure is quite similar to that of 120° spin rotation angle in a triangular lattice as observed in $CuCrO_2$ where the spin-dependent *d-p* hybridization is assumed to induce ferroelectric polarization along the screw axis except that the angle of rotation in our case is ∼133° [18,19,30,31]. These features suggest that the material $MnSb_2S_4$ could be a potential candidate to show spin-induced multiferroicity.

In this paper, we report the emergence of ferroelectric polarization below the helical spin ordering temperature ∼25 K in the monoclinic phase of $MnSb_2S_4$. Remarkably, the polarization is enhanced by six times when the applied magnetic field is at 9 T, indicating a strong magnetoelectric coupling. We suggest the inverse DM interaction as a possible mechanism for the occurrence of multiferroicity. This study provides another prototype example of spin-induced multiferroic in a nonoxide material possessing centrosymmetric monoclinic crystal structure.

II. EXPERIMENTAL DETAILS

$MnSb_2S_4$ was prepared by solid state reaction of stoichiometric mixture of elemental Mn, Sb, and S in an evacuated silica tube by heating at 500 °C for 5 days. The heated mixture was pressed into pellets and sintered at 500 °C for 10 days. Powder x-ray diffraction showed a trace amount of Sb_2S_3 impurity. Magnetic measurements were carried out with a Magnetic Property Measurement System superconducting quantum interference device (MPMS SQUID) magnetometer (Quantum Design, USA) and heat capacity was measured in a Physical Property Measurement System (PPMS). For the electrical measurements the samples were cut into thin plates and silver paste was applied as electrodes onto the wide faces. The dielectric constant was measured with the LCR meter (E4980A). To determine the electric polarization, we measured the pyroelectric current using a Keithley electrometer (6517A) with a constant rate of temperature sweep (10 K/min) and integrated it with time. To align the polar domains in the sample, a poling electric field was applied in the cooling process and removed at the lowest temperature and shorted for 30 min before the measurements of pyroelectric current. PPMS was used for the access of low temperatures and magnetic field.

III. RESULTS AND DISCUSSION

The crystal structure of $MnSb_2S_4$ is obtained from the refinement of x-ray data using the FULLPROF package with the monoclinic space group $C2/m$. The recorded x-ray diffraction data along with the refined data is shown in Fig. 1. From the refinement, approximately 3% of elemental sulfur impurity

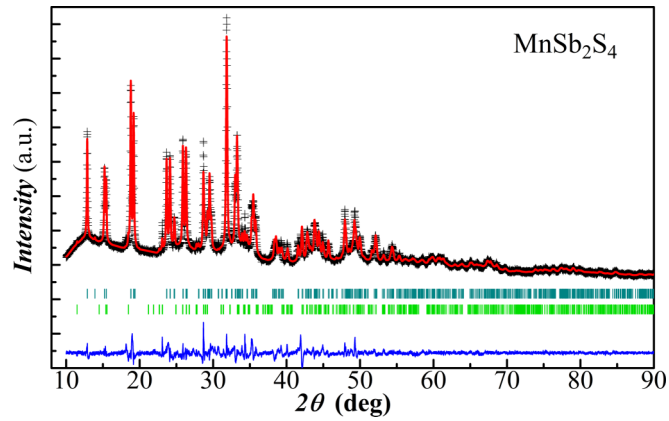

FIG. 1. X-ray diffraction pattern recorded at room temperature along with the Rietveld refinement data using $C2/m$ space group. The first and second row of tick marks indicates Bragg position of the main phase ($MnSb_2S_4$) and the impurity phase (elemental S), respectively. The bottom curve shows the difference between the recorded and fitted pattern.

was found in the sample. The lattice parameters, atomic positions, and overall refinement factors are displayed in the Supplemental Material [32]. The crystal structure obtained from the refined data is shown in Figs. 2(a) and 2(b) where we can see that the edge-shared MnS_6 octahedra are arranged in a chain along the *b* axis and the distorted SbS_5 square pyramid is alternatively attached to the MnS_6 octahedra. The chains are interconnected along the *a* axis and form layers along the *c* axis. The helicoidal spin structure of Mn^{2+} spins is drawn

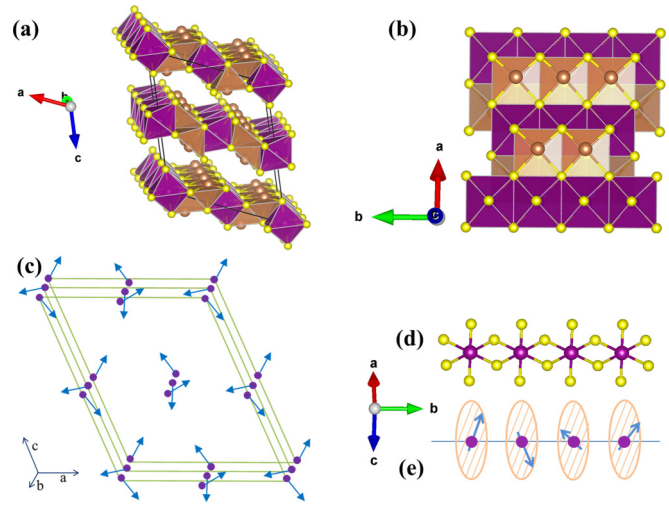

FIG. 2. (a) Crystal structure of $MnSb_2S_4$ as obtained from the refinement. The yellow spheres represent sulfur. The purple and yellow color polyhedral are corresponding to the MnS_6 octahedra and SbS_5 square pyramid. The MnS_6 octahedra make a chain along the *b* axis and SbS_5 are interlinked to the chain making layers along the *c* axis. (b) Crystal structure along the *c* axis showing the MnS_6 and SbS_5 polyhedra are connected in the *ab* plane. (c) Magnetic structure of Mn^{2+} ions drawn based on Ref. [27]. (d) Chain of Mn ions along *b* axis showing the edge sharing bond with S. (e) Chain of Mn spins along the *b* axis showing the spin helicity in the *ac* plane and propagation along the *b* axis.

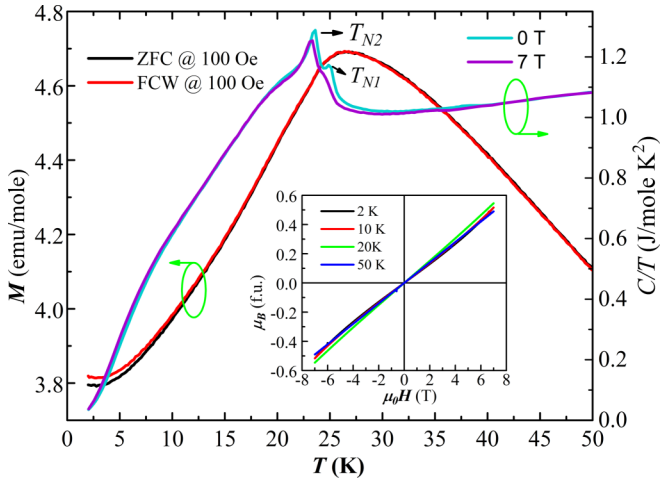

FIG. 3. Left axis shows the temperature dependence of DC magnetization measured under ZFC and FC condition. Right axis shows the heat capacity divided by temperature data. Inset shows the $M(H)$ curves measured at different temperatures.

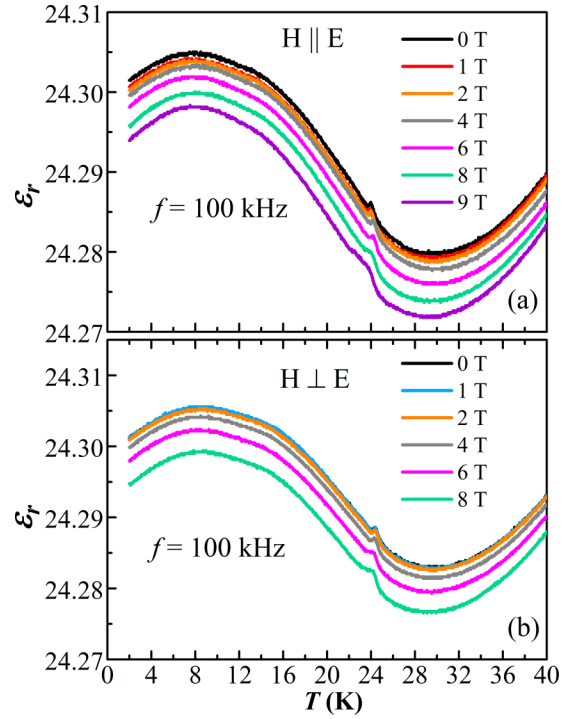

FIG. 4. Temperature dependence of dielectric constant measured from 2 to 40 K at 100 kHz in the presence of various magnetic field applied (a) parallel (b) perpendicular to the magnetic field.

in Fig. 2(c) according to Ref. [27]. A single chain of Mn ions along the b axis with an edge sharing bond of S is shown in Fig. 2(d). A schematic of helical Mn spins propagating along the b axis is shown in Fig. 2(e) according to Ref. [27].

Figure 3 shows the temperature dependence of zero-field-cooled (ZFC) and field-cooled (FC) magnetization at 100 Oe on the left axis and heat capacity divided by temperature on the right axis. The magnetization curve shows a maximum at 26 K indicating an antiferromagnetic transition. The magnetic behavior is similar to the earlier reported data, however, the monotonous decreasing trend of magnetization below the ordering temperature and the overlapping of ZFC and FC data compared to the earlier report suggest that there is no magnetic impurity present in our sample. The linear fit of inverse molar susceptibility versus temperature data estimates the μ_{eff} value as 6.02 μ_B, which is close to the theoretical value of Mn^{2+} ion moment 5.92 μ_B (shown in the Supplemental Material [32]). The obtained value of paramagnetic Curie temperature (θ_c) is −57 K and the calculated frustration parameter is $f = \frac{\theta_c}{T_N} \approx 2.3$ indicating the magnetic ordering is moderately frustrated. The zero-field heat capacity data (Fig. 3 right axis) shows two peaks ($T_{N1} = 25$ K and at $T_{N2} = 23.5$ K), which is in agreement with the previously reported data. At 7 T, the small peak at 25 K is suppressed and becomes a broad cusp. The nature of the peaks at T_{N1} and T_{N2} is discussed below based on phenomenological theory of phase transitions. The magnetization vs applied field recorded at various temperatures shows a nonlinear behavior below the ordering temperature such as 2, 10, and 20 K, and a linear behavior at 50 K (see inset of Fig. 3).

The temperature dependence of the dielectric permittivity (ε) was measured in the absence and presence of magnetic field for both the parallel ($H \parallel E$) and perpendicular ($H \perp E$) configurations and the results are shown in Figs. 4(a) and 4(b). A small kink type dielectric anomaly is evidenced near the magnetic ordering temperature ($T_{N2} \sim 24$ K) in the absence of magnetic field. With the application of magnetic field, the anomaly becomes broad and diffusive suggesting a magnetodielectric effect. Moreover, the presence of dielectric anomaly at the magnetic ordering temperature may be associated with possible ferroelectric transition concurrent with the magnetic ordering. The overall upturn feature of dielectric constant below 30 K may be related to the pretransitional magnetoelectric effect considering the quasi-two-dimensional character of magnetic network. A detailed temperature dependent magnetic structure determination is necessary to understand the dielectric behavior at low temperature.

The presence of a well-defined dielectric peak at the magnetic ordering temperature motivated us to perform the polarization measurements. In order to investigate the ferroelectric property we have poled the sample from 40 to 2 K with $E = 13$ kV/cm electric field and measured the pyroelectric current in the absence of electric field while warming the sample at 10 K/min rate. Like the dielectric measurement, the polarization is also measured in the presence of magnetic field for both $H \parallel E$ and $H \perp E$ configurations. A sharp asymmetric pyrocurrent peak was observed at the dielectric anomaly temperature in zero magnetic field. The polarizations obtained from the pyrocurrent measurements for $H \parallel E$ and $H \perp E$ are shown in Figs. 5(a) and 5(b), respectively. The subtle increment in the transition temperature in the pyrocurrent data can be due to the higher temperature sweeping rate. It should be mentioned that the polarization is switchable upon reversing the direction of electric field poling. Thus, the appearance of ferroelectric polarization at the magnetic ordering temperature indicates the spin induced ferroelectric polarization. The intrinsic nature of ferroelectric polarization is confirmed by the DC-biased current measurement where we see a consecutive polarization (positive) and depolarization

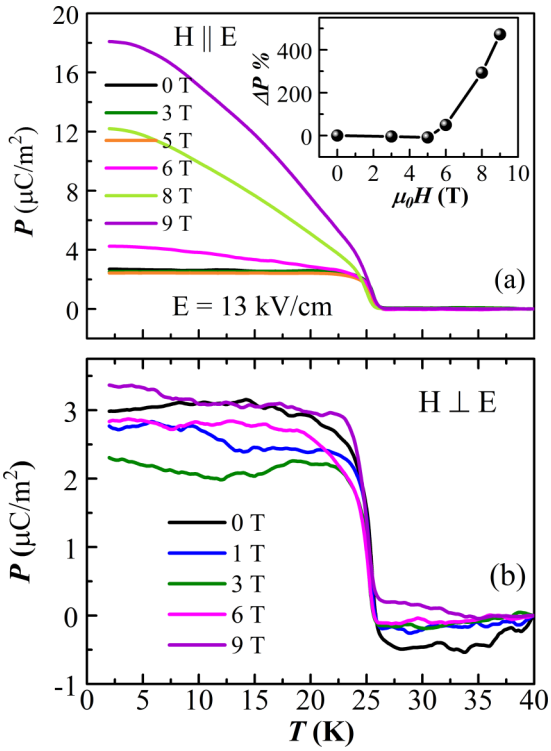

FIG. 5. Temperature evolution of electric polarization after integrating the pyrocurrent recorded after poling the sample from 40 to 2 K under $E = 13$ kV/cm and various magnetic field (a) parallel and (b) perpendicular to the electric field. Inset shows the magnetic field variation of electric polarization under parallel configuration.

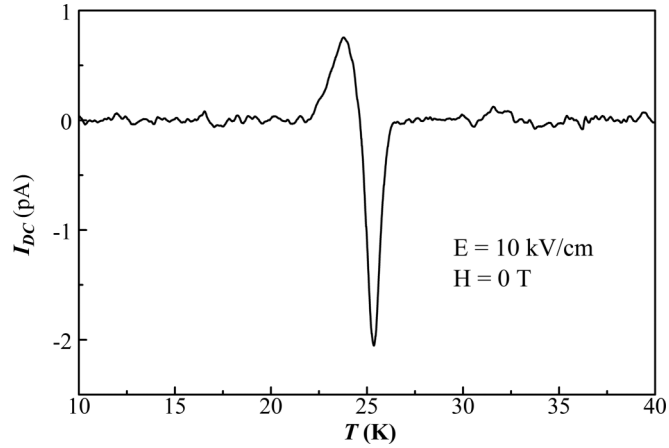

FIG. 6. DC-bias current measured after cooling the sample to 2 K without applying any electric field and measured while heating the sample under an electric field of 10 kV/cm.

(negative) peak at the ferroelectric ordering temperature while warming the sample in presence of electric field as depicted in Fig. 6 [33].

When magnetic field ($H \parallel E$) is applied, a remarkable increase ($\sim 500\%$) of polarization is observed above a critical magnetic field of about $H_{\rm crit} = 5$ T. At $H < H_{\rm crit}$ the polarization remains almost constant. A similar increase of polarization was observed in $CuCrO_2$ multiferroic but the enhancement of polarization is relatively low [19]. On the other hand, for $H \perp E$ configuration the polarization slightly decreases till 3 T and reverts back to a zero-field value with further increasing field [19]. This large anisotropic behavior of polarization also confirms the spin-driven ferroelectricity in this material.

The magnetically induced electric polarization in proper screw magnetic structures is usually interpreted using the single spin dependent *d-p* hybridization mechanism, which is considered to be valid, e.g., for delafossite compounds $CuFe_{1-x}Al_xO_2$ [30,31,34] and $ACrO_2$ ($A = $ Cu, Ag) with the proper screw and 120° rotation spin structure [19]. However, the Mn^{2+} ions in $MnSb_2S_4$ are located in centrosymmetric surroundings, which precludes single spin contributions to the magnetoelectric effect [35], although consideration of a cluster of several spins can give contribution to the magnetoelectric effect by the *d-p* hybridization mechanism [18].

From an earlier report [27], we infer that this compound has an incommensurate magnetic structure with one-dimensional (1D) propagation vector [0, 0.369, 0], which is the Λ point of the Brillouin zone and that is unchanged down to the lowest temperature [see Fig. 2(c)]. The magnetic structure was best fitted with a helicoidal model and can be described by two order parameters (a_1, a_2) and (b_1, b_2) transforming according to the irreducible representation (IR) Λ_2 and representing the components of magnetic moments along the x and z axes, respectively (here we assume the orthogonal axes x, y, and z to be along the axes a and b, and perpendicular to a and b, respectively). The magnetoelectric interaction has the form $I_y = (a_1b_2 - a_2b_1)P_y$. It can be shown that upon lowering the temperature the first magnetic phase transition at T_{N1} is into a sinusoidally modulated phase with magnetic moments lying in the ac plane, whereas the subsequent phase transition at T_{N2} results in a proper screw magnetic structure with electric polarization along the y axis in agreement with previous calculations [36]. Application of external magnetic field above $H_{\rm crit}$ arguably results in a flop of a spin rotation plane as to be perpendicular to the magnetic field. Thus, in the flopped magnetic structure an additional magnetic moment component along the y axis appears, which can be described by the order parameter (c_1, c_2) transforming according to IR Λ_1. The symmetry allows magnetoelectric interactions $I_{1\alpha} = (a_1c_2 - a_2c_1)P_\alpha$ and $I_{2\alpha} = (b_1c_2 - b_2c_1)P_\alpha$, where $\alpha = x, z$. A significant increase of electric polarization by magnetic field at $H \parallel E$ suggests that the coefficients at I_{1z} and I_{2x} in the thermodynamic potential expansion are significantly higher than at I_y, whereas practical independence of electric polarization at $H \perp E$ on magnetic field suggests that the coefficients at I_{1x} and I_{2z} are similar to that at I_y.

The magnetoelectric interactions given above can be expressed through spins. Denoting by $\vec{S}_1$ and $\vec{S}_2$ the spins of nearest Mn^{2+} ions adjacent along the b axis we obtain

$$I_y = (S_{1x}S_{2z} - S_{1z}S_{2x})P_y,$$
$$I_{1\alpha} = (S_{1x}S_{2y} - S_{1y}S_{2x})P_\alpha,$$
$$I_{2\alpha} = (S_{1z}S_{2y} - S_{1y}S_{2z})P_\alpha.$$

It appears that the components of magnetically induced electric polarization in this compound are proportional to the components of vector product of spins $\vec{S}_1 \times \vec{S}_2$ and are, thus,

due to the inverse DM interaction. The difference in electric polarization values for the $H \parallel E$ and $H \perp E$ cases in the magnetic field-induced phase can then be qualitatively understood as due to the qualitative differences in magnetoelectric interaction pairs I_{ix} and I_{iz} ($i = 1, 2$): one of the interactions gives rise to an electric polarization component normal to the plane of rotation of the spins, while the other one parallel to the rotation plane, and these components can differ in values. Single crystal measurements of magnetic field influence on electric polarization should provide further insight into the magnetoelectric interactions, however some predictions can be made based on the proposed theoretical description. Thus, an external magnetic field applied along the b axis should not change the electric polarization greatly but decrease it gradually with increasing field, as the plane of rotation of spins would not change and the magnetic moments would gradually align along the field direction. In contrast, application of external magnetic field in the ac plane should result in a flop of the spin rotation plane as to be perpendicular to the applied field above the critical field H_{crit}. This will result in the disappearance of electric polarization along the b axis, since $\vec{S}_1 \times \vec{S}_2$ will lie in the ac plane and $S_{1x}S_{2z} - S_{1z}S_{2x}$ will vanish, and the appearance of polarization in the ac plane, i.e., the electric polarization will flop from the b direction to the ac plane. The direction of electric polarization in the ac plane will be determined by the relative strengths of interactions $I_{1\alpha}$ and $I_{2\alpha}$. Thus, electric polarization will not necessary be parallel to the applied magnetic field but oriented at an angle. Detailed neutron diffraction experiment in the ground state as well as under magnetic field, as well as magnetoelectric measurements in various geometries are necessary in order to understand the magnetic field effect on polarization in more details.

In $MnSb_2S_4$ the Mn^{2+} ions are located in centrosymmetric positions, which forbids single spin-dependent contribution to magnetoelectric effect by any mechanism including the d-p hybridization. Indeed, the phenomenologically obtained interactions I_y, $I_{1\alpha}$, and $I_{2\alpha}$ are in accordance with local symmetry considerations revealing that in the zero-field proper screw magnetic structure electric polarization is parallel to the vector $\vec{e}_{ij}$ connecting two spins i and j if $\vec{e}_{ij} \parallel \vec{S}_i \times \vec{S}_j$ and if there is a twofold rotation axis along $\vec{e}_{ij}$ and a mirror plane perpendicular to it [22]. This can be considered as equivalent to the so-called ferroaxial mechanism used in some works for interpretation of electric polarization induction by proper screw magnetic structure [37,38], suggesting that chirality $\vec{e}_{ij} \cdot (\vec{S}_i \times \vec{S}_j)$ breaks inversion symmetry resulting in the emergence of polarization in the so-called ferroaxial crystal classes ($2/m$ in case of $MnSb_2S_4$). Microscopically the magnetoelectric interaction is similar to the inverse DM interaction. The sixfold increase of polarization in magnetic field in the studied sulphate, which arguably possesses stronger covalency than an ordinary oxide, reveals strong anisotropy of this interaction, possibly indicating strong influence of covalency effects. This can be used for further fundamental analysis of magnetoelectric interactions in general.

IV. CONCLUSIONS

In conclusion, a spin-driven ferroelectric polarization is observed in a centrosymmetric monoclinic compound $MnSb_2S_4$. Under magnetic field a sixfold enhancement of polarization is observed demonstrating a large magnetoelectric coupling. Appearance of electric polarization induced by proper screw spin ordering is explained using the inverse DM type interaction in accordance with local symmetry considerations. The finding of spin-induced ferroelectricity in this nonoxide material indicates the importance of helicoidal spin structure for the discovery of new multiferroics.

ACKNOWLEDGMENTS

The authors thank the International Centre for Materials Science (ICMS) and Sheik Saqr Laboratory (SSL) at Jawaharlal Nehru Centre for Advanced Scientific Research (JNCASR) for various experimental facilities. C.D. acknowledges JNCASR for providing research fellowship (JNC/S0248). N.V.T. acknowledges support by the Ministry of Education and Science of the Russian Federation (state assignment Grant No. 3.5710.2017/8.9).

[1] Y. Tokura, M. Kawasaki, and N. Nagaosa, Nat. Phys. **13**, 1056 (2017).
[2] H.Y. Hwang, Y. Iwasa, M. Kawasaki, B. Keimer, N. Nagaosa, and Y. Tokura, Nat. Mater. **11**, 103 (2012).
[3] M. Fiebig, J. Phys. D Appl. Phys. **38**, R123 (2005).
[4] M. Bibes and A. Barthélémy, Nat. Mater. **7**, 425 (2008).
[5] M. Fiebig, T. Lottermoser, D. Meier, and M. Trassin, Nat. Rev. Mater. **1**, 16046 (2016).
[6] M. M. Vopson, Crit. Rev. Solid State Mater. Sci. **40**, 223 (2015).
[7] Y. Tokura, S. Seki, and N. Nagaosa, Rep. Prog. Phys. **77**, 076501 (2014).
[8] S. Dong, J.-M. Liu, S.-W. Cheong, and Z. Ren, Adv. Phys. **64**, 519 (2015).
[9] T. Kimura, T. Goto, H. Shintani, K. Ishizaka, T. Arima, and Y. Tokura, Nature (London) **426**, 55 (2003).
[10] H. Katsura, N. Nagaosa, and A.V. Balatsky, Phys. Rev. Lett. **95**, 057205 (2005).
[11] I. A. Sergienko, C. Şen, and E. Dagotto, Phys. Rev. Lett. **97**, 227204 (2006).
[12] T. Kimura, Y. Sekio, H. Nakamura, T. Siegrist, and A. P. Ramirez, Nat. Mater. **7**, 291 (2008).
[13] T. Kimura, Annu. Rev. Condens. Matter Phys. **3**, 93 (2012).
[14] G. Lawes, A. B. Harris, T. Kimura, N. Rogado, R. J. Cava, A. Aharony, O. Entin-Wohlman, T. Yildirim, M. Kenzelmann, C. Broholm, and A. P. Ramirez, Phys. Rev. Lett. **95**, 087205 (2005).
[15] S. Ishiwata, Y. Taguchi, H. Murakawa, Y. Onose, and Y. Tokura, Science **319**, 1643 (2008).
[16] S. Ishiwata, Y. Kaneko, Y. Tokunaga, Y. Taguchi, T.-h. Arima, and Y. Tokura, Phys. Rev. B **81**, 100411 (2010).

[17] M. Collins and O. Petrenko, Can. J. Phys. **75**, 605 (1997).
[18] T.-h. Arima, J. Phys. Soc. Jpn. **76**, 073702 (2007).
[19] S. Seki, Y. Onose, and Y. Tokura, Phys. Rev. Lett. **101**, 067204 (2008).
[20] T. Kurumaji, S. Seki, S. Ishiwata, H. Murakawa, Y. Tokunaga, Y. Kaneko, and Y. Tokura, Phys. Rev. Lett. **106**, 167206 (2011).
[21] M. Kenzelmann, G. Lawes, A. B. Harris, G. Gasparovic, C. Broholm, A. P. Ramirez, G. A. Jorge, M. Jaime, S. Park, Q. Huang *et al.*, Phys. Rev. Lett. **98**, 267205 (2007).
[22] T. A. Kaplan and S. D. Mahanti, Phys. Rev. B **83**, 174432 (2011).
[23] H. Murakawa, Y. Onose, K. Ohgushi, S. Ishiwata, and Y. Tokura, J. Phys. Soc. Jpn. **77**, 043709 (2008).
[24] S. Seki, X. Yu, S. Ishiwata, and Y. Tokura, Science **336**, 198 (2012).
[25] E. Ruff, S. Widmann, P. Lunkenheimer, V. Tsurkan, S. Bordács, I. Kézsmárki, and A. Loidl, Sci. Adv. **1**, e1500916 (2015).
[26] K. Singh, A. Maignan, C. Martin, and C. Simon, Chem. Mater. **21**, 5007 (2009).
[27] P. Léone, C. Doussier-Brochard, G. André, and Y. Moëlo, Phys. Chem. Miner. **35**, 201 (2008).
[28] S. F. Matar, R. Weihrich, D. Kurowsky, A. Pfitzner, and V. Eyert, Phys. Rev. B **71**, 235207 (2005).
[29] A. Pfitzner and D. Kurowski, Z. Kristallogr. Cryst. Mater. **215**, 373 (2000).
[30] T. Kimura, J. C. Lashley, and A. Ramirez, Phys. Rev. B **73**, 220401 (2006).
[31] S. Seki, Y. Yamasaki, Y. Shiomi, S. Iguchi, Y. Onose, and Y. Tokura, Phys. Rev. B **75**, 100403 (2007).
[32] See Supplemental Material at http://link.aps.org/supplemental/10.1103/PhysRevB.98.174430 for structural parameters, magnetic susceptibility, and magnetodielectric effect.
[33] C. De, S. Ghara, and A. Sundaresan, Solid State Commun. **205**, 61 (2015).
[34] T. Nakajima, S. Mitsuda, S. Kanetsuki, K. Tanaka, K. Fujii, N. Terada, M. Soda, M. Matsuura, and K. Hirota, Phys. Rev. B **77**, 052401 (2008).
[35] M. Matsumoto, K. Chimata, and M. Koga, J. Phys. Soc. Jpn. **86**, 034704 (2017).
[36] C. Tian, C. Lee, E. Kan, F. Wu, and M.-H. Whangbo, Inorg. Chem. **49**, 10956 (2010).
[37] R. D. Johnson, S. Nair, L. C. Chapon, A. Bombardi, C. Vecchini, D. Prabhakaran, A. T. Boothroyd, and P. G. Radaelli, Phys. Rev. Lett. **107**, 137205 (2011).
[38] R. D. Johnson, L. C. Chapon, D. D. Khalyavin, P. Manuel, P. G. Radaelli, and C. Martin, Phys. Rev. Lett. **108**, 067201 (2012).